Journal of Physics: Conference Series **71** (2007) 012008 doi:10.1088/1742-6596/71/1/012008

Effects of fast neutral particles in low-pressure gas discharges

Z. Donkó, P. Hartmann, K. Kutasi

Research Institute for Solid State Physics and Optics of the Hungarian Academy of Sciences, H-1525 Budapest POB 49, Hungary

E-mail: donko@sunserv.kfki.hu

Abstract. The effects of fast neutral (heavy) particles on the characteristics of low-pressure noble gas discharges are reviewed. Complementing experimental observations, numerical simulations are applied to demonstrate the importance of these species in the (i) surface reactions causing cathodic electron emission and (ii) gas-phase reactions leading to the creation of charged particles and to light emission through excitation processes. All these processes are found to be important at high values of the electric field to gas density ratio, E/n, under which conditions positive ions – being the primary species creating fast neutrals in collision processes – acquire high energy in the cathode region.

1. Introduction

It has widely been accepted that the basic characteristics of low-pressure noble gas discharges can be understood by considering only electrons and ions as "active" particles in the discharge plasma. Thus most of the discharge models operate with these two types of charged particles, and these models have indeed successfully explained many of the phenomena, which are of primary importance in gas discharge physics (e.g. breakdown of the gas, spatial structure of glow discharges, basic features of light emission distribution, as well as electrical characteristics). Ionization in such models is assumed exclusively due to electron impact (traditionally called as the "α process") and secondary electron emission is assumed solely due to positive ions arriving at the cathode (traditionally called as the "γ process").

Clearly, some of the theories (based on the electron-ion picture) are only valid for a limited range of discharge conditions, and it has been recognized long ago that under some circumstances additional types of particles and/or elementary processes may have an important role. As a famous example, the specific shape of the Paschen curve of helium (see e.g. [1]) may be mentioned; in order to explain the experimentally observed behavior, an ionization term by fast heavy particles had to be included in the theory. Townsend's theory of breakdown has further been revised in the past years by studies of Phelps and Petrović [2], who have carefully analyzed the effects of various gas-phase and surface elementary processes. Besides gas-phase processes induced by the ions accelerated in the electric field, Ref. [2] also considered the *fast neutral atoms* originating from the collisions between fast ions and background (thermal) gas atoms. Moreover, besides that induced by positive ions, additional electron emission from the cathode due to ultraviolet photons, metastable atoms and fast neutrals have also been taken into account in [2], and the combination of modeling with the analysis of extensive published experimental

data made it possible to uncover the roles played by the above processes at different discharge conditions.

As excitation processes lead to light emission, in optically thin plasmas the spatial distribution of light emission may provide direct information about the different excitation processes. As expected at high values of the reduced electric field (electric field to gas density ratio) E/n [2], studies of light emission distributions in Towsend discharges have demonstrated excitation caused by heavy particles [3]. As regards to glow discharges, it is well-known that near/at the cathode bright light emission is observed at high E/n conditions. This light emission, often termed as "cathode glow" originates mainly from fast neutral-impact excitation. The spectral composition of the cathode glow and the negative glow (caused by the impact excitation of electrons that acquire high energy during their flight through the cathode sheath) may differ significantly [4], as the cross sections for a given atomic transition are generally different for excitation by electrons and fast neutrals. It is noted that while cross sections for electron impact excitation of noble gases can be considered as well established ones, cross sections for fast heavy particles are only known in a limited number of cases [5, 6, 7]. Thus models which include heavy-particle effects are inherently limited in their accuracy due to the uncertainties of the input data.

It is to be mentioned that besides inducing electron emission from the cathode and light emission near the cathode at high E/n conditions, fast atoms and fast ions also play a role in the (i) heating of the background gas and (ii) the sputtering of the cathode material. Heating of the gas occurs through the thermalization of fast heavy particles in collisions with the background gas atoms [8, 9, 10] and may change some of the discharge characteristics due to the local rarefication of the gas (which is a consequence of the increase of the temperature) [11]. The other effect mentioned above, the sputtering of the cathode, is a very important process, and serves as the basis for a series of applications, ranging from hollow cathode lasers [12, 13, 14] and spectral lamps [15], to glow discharge spectroscopy, where samples to be analyzed are connected as cathode and the discharge plasma created over their surface is analyzed by optical emission or mass spectroscopy [16].

In this paper we review some of the experimental and modeling results regarding the effects of heavy particles (i) *on gas breakdown and self-sustainment of discharges operated at high voltages (in the kV regime)*, as well as (ii) *on light emission characteristics of low-pressure discharges.* Following a brief description of the modeling approach in section 2, section 3 reviews some earlier representative experimental data, as well as our combined experimental and modeling studies on these phenomena. Section 4 gives the conclusions of the paper.

2. Simulation models

The non-hydrodynamic transport of the fast species in the discharges investigated here requires a kinetic approach for the fast species as their collision free path may be comparable to device dimensions [17]; due to its flexibility we chose Monte Carlo (MC) simulation for this purpose. We use two different computational approaches in our studies presented here. In the study of the breakdown of helium gas, where the electric field is homogeneous, we apply a full Monte Carlo simulation to follow the motion of all electrons, positive ions, as well as fast atoms in the electrode gap. In the other studies, where well-developed glow discharges are considered, we apply a one-dimensional heavy-particle hybrid model [8, 18, 19, 20, 21] which combines the fluid description of positive ions and slow electrons with kinetic description of fast plasma species: fast electrons, argon ions and fast neutral atoms. For the slow electrons, which are no longer able to ionize the gas, the hydrodynamic treatment is sufficiently accurate, so these electrons can be described by a fluid model. The hybrid models used here consists of the following parts:

- a two-component fluid module for positive ions and slow electrons,

- Monte Carlo simulation modules for fast electrons, argon ions and fast neutral atoms (to obtain accurate ionization source functions, fluxes and energy distributions of ions and fast neutrals at the cathode surface, as well as spatial distribution of the excitation rate), and
- additional modules for the calculation of the gas temperature distribution in the discharge gap, as well as for the calculation of the apparent electron emission coefficient of the cathode.

The interconnection of these "modules" is sketched in figure 1. The fluid model accounts for the balance and transport of positive ions and slow electrons. It makes use of the source functions of these species in the determination of their density distributions. Besides this, the fluid part delivers the potential distribution in the discharge, based on the potentials of the electrodes and the charge density distributions. This potential distribution is transferred to the MC simulation modules of the different charged species. The MC modules provide the source functions of charged particles, which are fed back to the fluid model. Additionally, the energies of the particles falling onto the cathode surface (as calculated in the MC modules for ions and fast neutrals) are used in the calculation of the apparent electron yield. These latter two MC modules also provide the heating terms, which are needed in the calculation of the gas temperature distribution. The calculated gas temperature profile (which actually results in a space-dependent buffer gas density distribution) is coupled back to the fluid module, as well as to all the three MC modules.

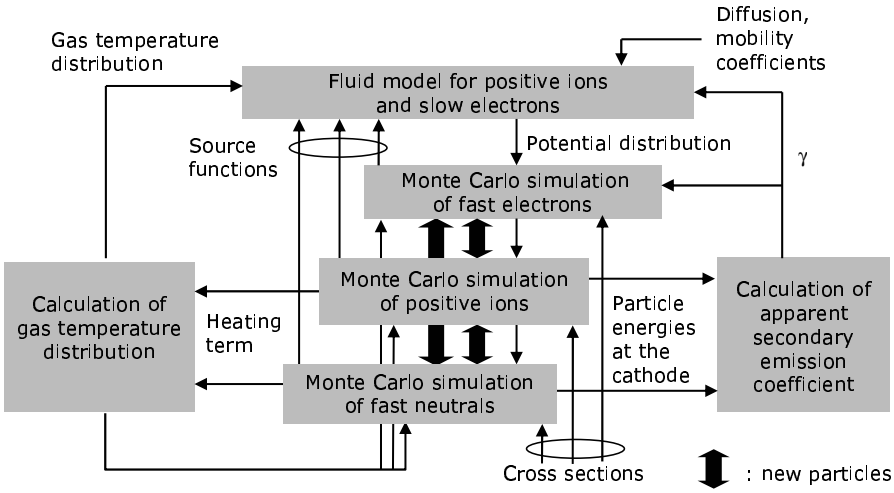

Figure 1. The scheme of the heavy-particle hybrid model.

In the following we first review the elementary processes considered in the model. Subsequently we introduce the concept of the apparent electron yield at the cathode and outline its calculation. Subsequently we briefly describe the parts of the model listed above. In the models applied here molecular ion formation and recombination processes are neglected, as well as the backscattering of electrons from the anode. In our one-dimensional treatment the electrodes are assumed to be infinite, plane and parallel. Cathode sputtering is not taken into account due to the relatively low values of the reduced current density.

2.1. Elementary processes in the gas phase

In the gas phase we take into account elastic, excitation and ionization collision processes of electrons, positive ions and fast gas atoms with the background gas. The processes are listed in Table 1.

The scattering of electrons in elastic momentum transfer and excitation collisions is assumed to be isotropic. In the case of electron impact ionization, the energies of the scattered and

Table 1. Gas-phase elementary processes considered in the model. Note: X denotes the filling gas (He or Ar in our case), X^* and X^F are excited and fast atoms, respectively.

No.	Process	Process name
1.	$e + X \rightarrow e + X$	elastic collision
2.	$e + X \rightarrow e + X^*$	excitation
3.	$e + X \rightarrow e + e + X^+$	ionization
4.	$X^+ + X \rightarrow X^+ + X^F$	elastic collision (isotropic part)
5.	$X^+ + X \rightarrow X^+ + X^F$	elastic collision (backward part)
6.	$X^+ + X \rightarrow X^+ + X^{*F}$	excitation
7.	$X^+ + X \rightarrow X^+ + X^+ + e$	ionization
8.	$X^F + X \rightarrow X^F + X^F$	elastic collision
9.	$X^F + X \rightarrow X^F + X^{*F}$	excitation
10.	$X^F + X \rightarrow X^F + X^+ + e$	ionization

ejected electrons, and the directions of their velocity vectors are calculated in accordance with the procedures described in Refs. [22, 23, 24]. The cross section of the isotropic part of the elastic $X^+ + X$ collisions (Q_i) is taken from Ref. [5, 25], while the charge transfer cross section (backward part of elastic scattering, Q_b) is obtained from the momentum transfer cross section (Q_m) as $Q_b = (Q_m - Q_i)/2$ [25]. In isotropic collisions the scattering and azimuth angles are chosen to reflect isotropic scattering in the center-of-mass (COM) system. The energy sharing of the collision partners is determined from the scattering angles, see e.g. [26]. The cross section of the elastic $X^F + X$ collision in isotropic approximation is $Q_i^a = (3/2)Q_v$, where Q_v is the viscosity cross section [5]. The calculation of scattering angles and energy sharing is carried out in the same way as in the case of $X^+ + X$ collisions. The scattering of particles in inelastic heavy particle collisions is assumed to be isotropic in the COM system.

The charge and momentum transfer collisions of heavy particles create fast atoms that play a dominant role in the heating of the gas and the sputtering of the cathode [27]. In the Monte Carlo modules the ions and fast atoms are traced until they reach the cathode surface or – in the case of fast atoms – their energy falls below a threshold energy (ε_{th}, see later) when they can be considered thermalized. This way the energy of each of the fast atoms and positive ions, upon arrival to the cathode surface can be calculated. Besides the ions created in the cathode sheath, the flux of ions arriving from the negative glow is also taken into account.

2.2. Elementary processes at the cathode surface and the effective electron yield

Most of the gas discharge models consider only ion-induced secondary electrons, but this approximation cannot be regarded as strictly correct for most of the possible conditions [2]. For the discharge conditions covered here, secondary emission due to fast neutrals is also expected to be a significant process.

In our "heavy-particle" hybrid models, besides those of the electrons, we also follow the trajectories of individual ions and fast neutrals in the cathode region. The information provided by such an approach makes it possible to derive an "apparent electron yield" at the cathode, which is the ratio of the electron to ion current density, $\gamma = (j^-/j^+)_{cathode}$. Let N_i and N_a denote the number of ions and fast atoms arriving to the cathode due to the emission of N_0 primary electrons from the cathode. In stationary state, to ensure that the discharge is self-sustained, these ions and fast atoms have to induce the emission of N_0 "new" electrons from the

cathode, i.e.:

$$\sum_{k=1}^{N_\mathrm{i}} \gamma_\mathrm{i}(\varepsilon_k) + \sum_{k=1}^{N_\mathrm{a}} \gamma_\mathrm{a}(\varepsilon_k) = N_0 \tag{1}$$

holds, where $\gamma_\mathrm{i}(\varepsilon)$ and $\gamma_\mathrm{a}(\varepsilon)$ are the energy-dependent secondary electron yields (probabilities that an electron is emitted from the cathode due to the impact of a positive ion or a fast atom) and ε_k is the energy of the k-th ion or atom. The ratio of the electron to the ion current density at the cathode (being itself the apparent γ) equals to the ratio N_0/N_i, which defines the way to determine γ [10]:

$$\gamma = \frac{\sum_{k=1}^{N_\mathrm{i}} \gamma_\mathrm{i}(\varepsilon_k) + \sum_{k=1}^{N_\mathrm{a}} \gamma_\mathrm{a}(\varepsilon_k)}{N_\mathrm{i}}. \tag{2}$$

It is noted that the data we use characterize "practical" or "dirty" cathode surfaces for which the electron yields can be significantly different compared to those obtained using ion beam experiments with heavily sputtered samples in ultrahigh vacuum environment (for more details on this topic see Ref. [2]).

2.3. Hybrid model

The principal variables of the fluid model are the positive ion and slow electron densities, $n_\mathrm{i}(x)$ and $n_\mathrm{e}(x)$, and the electric potential $V(x)$. These variables can be calculated self-consistently from the continuity and momentum transfer equations for the charged species, and the Poisson equation (e.g. [28, 29]):

$$\frac{\partial n_\mathrm{i}}{\partial t} + \frac{\partial (n_\mathrm{i}\mathbf{v}_\mathrm{i})}{\partial x} = S_\mathrm{i}, \qquad \frac{\partial n_\mathrm{e}}{\partial t} + \frac{\partial (n_\mathrm{e}\mathbf{v}_\mathrm{e})}{\partial x} = S_\mathrm{e}, \tag{3}$$

$$n_\mathrm{i}\mathbf{v}_\mathrm{i} = n_\mathrm{i}\mu_\mathrm{i}\mathbf{E} - \frac{\partial (n_\mathrm{i}D_\mathrm{i})}{\partial x}, \qquad n_\mathrm{e}\mathbf{v}_\mathrm{e} = -n_\mathrm{e}\mu_\mathrm{e}\mathbf{E} - \frac{\partial (n_\mathrm{e}D_\mathrm{e})}{\partial x}, \tag{4}$$

$$\frac{\mathrm{d}V}{\mathrm{d}x} = -\frac{e}{\epsilon_0}(n_\mathrm{i} - n_\mathrm{e}), \tag{5}$$

where $\mathbf{v}_\mathrm{e}$ and $\mathbf{v}_\mathrm{i}$ are the mean velocities, S_e and S_i are the source functions, μ_e and μ_i are the mobilities, and D_e and D_i are the diffusion coefficients of slow electrons and ions, respectively, e is the elementary charge, and ϵ_0 is the permittivity of free space. For details regarding the values of the above transport coefficients used in the studies presented in this review, the Reader is referred to the original papers cited in the forthcoming sections, while discussions of some of the assumptions concerning these values can be found in [30, 31].

In the solution of the above set of equations the source functions of ions and electrons are taken from Monte Carlo (MC) simulation of the fast electrons. Those electrons which lose their energy in the negative glow and are no longer able to produce any additional ionization, are transferred from the MC simulation to the slow electron group in the fluid model. The fluid and the Monte Carlo modules of the simulation are carried out iteratively to reach the stationary solutions of the investigated problems.

2.4. Calculation of the gas temperature

The gas temperature distribution $T_\mathrm{g}(x)$ is calculated similarly to that described in [8]. The heat conductivity equation:

$$\frac{\mathrm{d}^2 T_\mathrm{g}(x)}{\mathrm{d}x^2} + \frac{P(x)}{\kappa} = 0, \tag{6}$$

where $P(x)$ is the gas heating source term and κ is the thermal conductivity of the gas (κ = 0.0177 W m^{-1} K^{-1} for argon, and κ = 0.143 W m^{-1} K^{-1} for helium), is solved with the boundary conditions [8]:

(i) fixed anode temperature, T_a, and

(ii) specified temperature gradient in front of the cathode:

$$\kappa \left| \frac{\mathrm{d}T}{\mathrm{d}x} \right|_{\mathrm{cathode}} = \frac{2\alpha}{2-\alpha} C_\mathrm{p} m_\mathrm{p} \Delta T_\mathrm{s} \frac{n_\mathrm{s} v_\mathrm{s}}{4}, \tag{7}$$

where α is the thermal accommodation coefficient, C_p is the specific heat of the gas at constant pressure, m_p, n_s and v_s are the mass, the density, and the average thermal velocity of the gas atoms in front of the cathode, respectively, and ΔT_s is the "temperature jump" at the cathode surface, i.e. the difference of the cathode temperature T_c and the gas temperature in front of the cathode T_s.

The thermal accommodation coefficient α describes the extent of energy exchange between the cathode and the slow particles colliding with it. At $\alpha = 1$ the backscattered particles attain the temperature of the cathode, while at $\alpha = 0$ no energy exchange occurs during the reflection. For the interaction of fast particles (that can have up to several hundred eV energy in the cathode sheath) with the cathode surface different assumptions are used in the modeling literature. Here we assume that particles are reflected from the cathode with a fraction of their kinetic energy. This fraction is derived from the data of [32] and [33]. A previous work [10] has demonstrated that the reflected particles (fast atoms and fast neutralized ions) dominate in the heating of the gas, thus their effect cannot be neglected (as done in several studies). The gas heating term $P(x)$ – arising from the thermalization of fast heavy particles – is calculated according to the procedures described in [20]; the threshold energy for which a particle is considered to be thermalized is chosen to be 9 times the average thermal energy of buffer gas atoms, $\varepsilon_\mathrm{th} = 9 \times (3/2) k T_\mathrm{g}(x)$.

3. Results and discussion

3.1. Breakdown of low-pressure helium gas

The breakdown of gases – being one of the most fundamental phenomena in gas discharge physics – has been investigated since the very beginning of gas discharge research and still attracts continuous interest [34, 35, 36, 37, 38, 39]. Apart from the theoretical interest, the starting processes of the gas discharge have importance in a wide range of applications. The breakdown of the gas is also a crucial process in electric insulation where it is to be avoided.

For plane-parallel electrode arrangements the Paschen law (see e.g. [1]) states that the breakdown voltage is a function of the product of gas pressure (p) and electrode separation (d), $V_\mathrm{BR} = f(pd)$. The Paschen curve always exhibits a minimum: both the $(pd)_\mathrm{min}$ value where the minimum is found and the minimum breakdown voltage $V_\mathrm{BR}^\mathrm{min}$ are characteristic for the pair of the gas and cathode material. The Paschen curve of helium, on the other hand, has a particular shape in comparison with many other gases, see figure 2(a). Point "A" indicates the Paschen minimum, while "B" and "C" correspond to the characteristic turning points of the curve. Penning has found that at low pressures (below $pd \approx 220$ Pa cm) breakdown may occur at three different values of the voltage [34]. Besides helium, this type of behavior was also observed in mercury vapor (see e.g. [37]). In previous works several attempts have been made to explain the shape of Paschen curve of helium [1, 34, 35, 37]; it is generally accepted that the energy dependence of the γ_i coefficient (electron emission yield for ion impact onto the cathode surface) and the ion impact ionization of buffer gas atoms ($\mathrm{He}^+ + \mathrm{He} \rightarrow \mathrm{He}^+ + \mathrm{He}^+ + \mathrm{e}^-$) are responsible for the curve shape at low pressures.

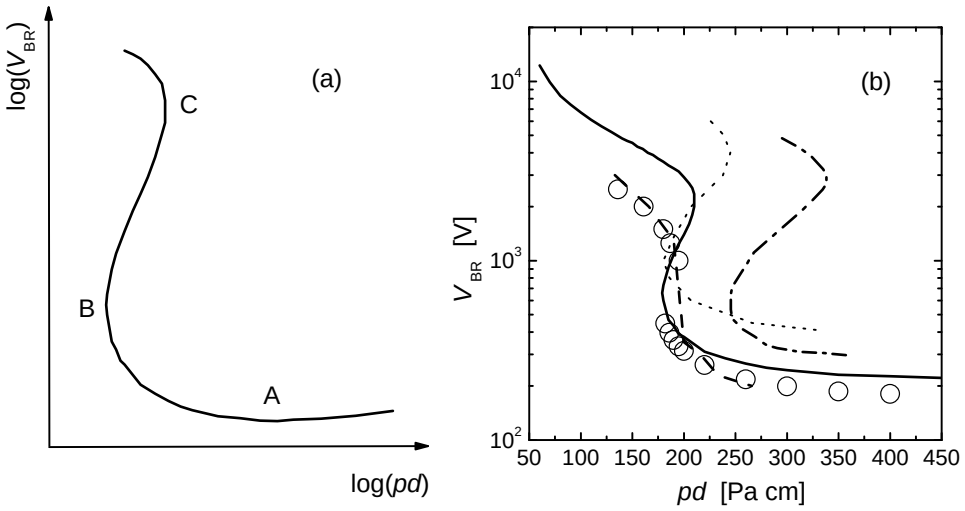

Figure 2. (a) Schematic representation of the Paschen curve of helium. Point "A" indicates the Paschen minimum, while "B" and "C" denote the characteristic turning points. (b) The result of our simulation (——) in comparison with the results of · - · Penning [34], - - - Jelenković and Phelps [39], ··· Guseva [37], and our experimental results (○).

We have carried out both experimental and simulation studies on the breakdown of helium at low pressures. In the experiment we have measured the breakdown voltage of helium gas between plane and parallel electrodes, made of copper, and positioned at a fixed distance of $d = 1$ cm, in the voltage range up to $V_{\rm BR} = 2500$ V [40]. In figure 2(b) the results of these measurements are presented together with earlier experimental data, and with the Paschen curve calculated from our model, up to $V_{\rm BR} \approx 10^4$ V. Our simulations use the cross sections from [41, 42] for electron induced collisions, for He^+ ions and fast He atoms we use data published in [43, 44, 45, 46, 47, 48], while for surface processes data are taken from [49, 50, 51, 52].

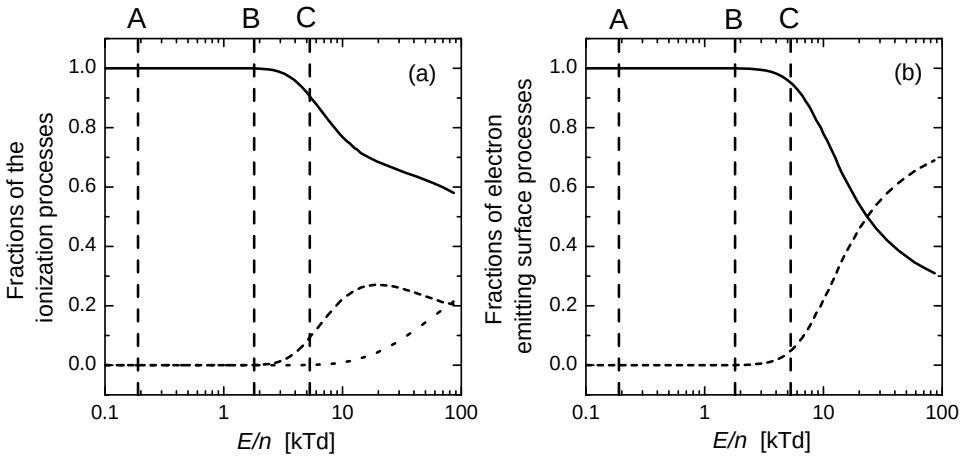

Figure 3. (a) Fractions of ionization processes: —— electron impact ionization, - - - ion impact ionization, ··· atom impact ionization; (b) Fractions of primary-electron emitting surface processes: —— ion impact electron emission, - - - atom impact electron emission. "A", "B" and "C" are the characteristic points of the Paschen curve shown in figure 2(a).

The particular shape of the Paschen curve can be understood by analyzing the processes responsible for the charge reproduction. In figure 3(a) the contributions of the different (electron, ion and fast atom impact) ionizing processes to the total ion production are displayed. Figure 3(b) shows the contributions of the positive ions and of the neutral atoms to the emission of primary electrons from the cathode. Both these data sets are given as a function of the reduced electric field E/n along the calculated Paschen curve, as they are not unique functions of the gas pressure. The results of the simulations show that on the "A"–"B" section of the Paschen curve (and at higher pressures from point "A", see figure 2(a)) the only important processes in the self-maintenance of the discharge are the electron impact ionization and the electron emission from the cathode due to He^+ impact. The Paschen minimum $(pd)_{\min}$ found experimentally corresponds to $E/n = 0.13$ kTd, where 1 kTd = 10^{-18} Vm^2. On the "B"–"C" section of the curve the electron impact ionization still dominates in the production of ions. The E/n values corresponding to points "B" and "C" are 1.5 kTd and 4.3 kTd, respectively. The number of ions produced by a primary electron decreases with increasing voltage, but the increase of γ_i with the kinetic energy of the ions compensates for this. With further increasing voltage – above point "C" – electron emission from cathode due to fast He atoms plays an important role, as it can bee seen in figure 3(b). This process already accounts for ≈ 20 % of primary electron production at $V = 4000$ V ($E/n \cong 10$ kTd). At these conditions positive ion impact causes ≈ 25 % of the ionization, while fast He atoms have only a share of 1 %. On the "right hand side" of the Paschen curve (at pressures higher than that corresponding to the Paschen minimum $(pd)_{\min}$, point "A" in figure 2(a)) the breakdown voltage slowly increases with increasing pressure. This increase is attributed to the fact that with increasing pressure gradually more electron energy is deposited into excitation.

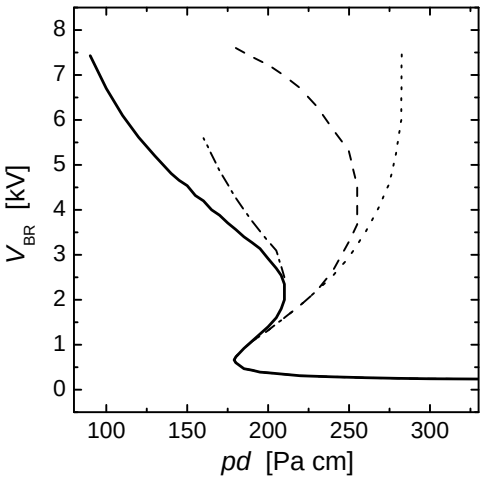

Figure 4. Comparison of different models: — full simulation, · - · ignoring fast atoms, - - - ignoring ion impact ionization, ··· ignoring fast atoms and ion impact ionization.

To investigate the overall effect of certain elementary processes on the shape of the Paschen curve, we also carried out simulations in which we ignored some of the processes. Together with the results of the simulations including all the elementary processes listed in Table, figure 3 shows the Paschen curves obtained by neglecting: (i) processes initiated by fast neutral atoms, (ii) ionization by ion impact, and (iii) both of the above processes. The results shown in figure 4 indicate that below ≈ 1000 V the processes ignored have no effect on the breakdown voltage. At higher voltages, however, both the fast atom initiated processes and He^+ impact ionization have a significant effect on the breakdown voltage. All these observations are in agreement with earlier explanations of the shape of the Paschen curve in helium, except that we also identify the electron emission due to fast neutral bombardment of the cathode as an important process.

3.2. Self-sustainment of high-voltage helium discharges

The phenomena taking place in abnormal DC glow discharges – usually operating in the ~ 100 Pa pressure range at a voltage of few hundred Volts – have thoroughly been investigated during the past decades. On the other hand, low-pressure glow discharges operating at more extreme conditions, e.g. at voltages of several thousand Volts, have rarely been studied by self-consistent models. Such discharges have important applications, e.g. as high-current electron guns. The experimental investigations (performed at Shizuoka University, Japan) [53, 54] of the discharge arrangement studied in this section (equipped with a concave cathode) have indeed been motivated by this application [55]. The experimental discharge arrangement consists of parallel ≈ 10 cm-diameter disk electrodes made of aluminium, to minimize cathode sputtering. The discharge has been operated in helium at pressures between 3 Pa and 30 Pa, at electrode separations of 20 – 30 cm, and voltages ranging from 1 kV to 5 kV. The voltage - current - pressure characteristics of the discharge, the potential distribution in the gap, and the energy distribution of fast electrons at the anode have been determined experimentally [53, 54]. The experiments have also shown that the properties of the discharges with plane and concave cathodes are very similar, except for the focusing of the beam of fast electrons in the case of the concave cathode.

Here we analyze through simulations [56] the importance of individual elementary processes and the self-maintenance mechanism (processes of charge reproduction) of this high-voltage discharge. The required input data (cross sections) for electron-induced collisions are taken from [41, 42]. For cross sections of He^+ ions and fast He atoms we use data published in [5, 44, 45, 47, 48] while data regarding surface processes are taken from [49, 50, 51, 52].

The results of the calculations are presented for a constant electrode separation $L = 28$ cm, a voltage of $V = 4000$ V, and for three values of current: $I = 1$ mA, 5 mA, and 20 mA. Due to small uncertainties in pressure measurement in the experiment we adjust the gas pressure in the calculations in a way that the calculated values of current match the experimental ones. The calculated values of the pressure for the three current values indicated above are $p = 3.6$ Pa, 5.0 Pa, and 7.6 Pa, which are in a reasonable agreement with the experimental values of 3.8 Pa, 5.5 Pa, and 8.1 Pa.

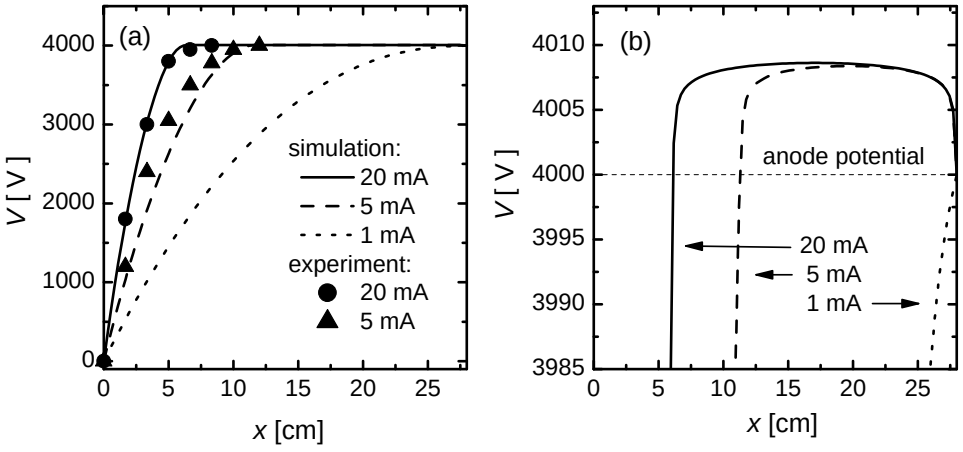

Figure 5. (a) Calculated (lines) and measured (symbols) potential distribution in the discharges at $V = 4000$ V, $L = 28$ cm and $I = 1$, 5, and 20 mA. The cathode is situated at $x = 0$ cm, while the anode is at $x = 28$ cm. (b) Potential distribution in the negative glow. (The horizontal dashed line shows the anode potential.)

Figure 5(a) shows the potential distribution between the electrodes, for $I = 1$, 5, and

20 mA. The $V(x)$ curves clearly show the cathode sheath – negative glow structure of the discharges operated at 5 mA and 20 mA. For these conditions the potential distribution is closely parabolic at the cathode side of the gap. The cathode sheath has a length (determined from the extrapolation of the linearly falling part of $E(x)$ to zero field), $d_c \approx 10$ cm and 6 cm, respectively, for the above values of the current. The space beyond the cathode sheath is filled by the negative glow. At $I = 1$ mA the cathode sheath occupies the whole discharge region, there is no space for the formation of the negative glow: the discharge gets obstructed [57].

At the higher values of the current (5 mA and 20 mA) the simulations show the existence of an electric field reversal in the negative glow part of the discharge. The enlarged part of the potential distribution, displayed in figure 5(b), shows a plasma potential ≈ 8 V higher than the anode potential. The position of the field reversal (which coincides with the position of the maximum of the potential) is located at $d_f = 19.7$ cm, and 17.2 cm, respectively, for $I = 5$ and 20 mA. We find that for these values of the current the field reversal position is situated halfway between the position of the sheath–glow boundary and the anode. This behavior is in excellent agreement with the predictions of the analytical model of [58]. Experimental data for the potential, measured by emissive probe technique [59], for the $I = 5$ and 20 mA cases are also plotted in figure 5(a). The results of the calculations are in a fair agreement with the experimental data.

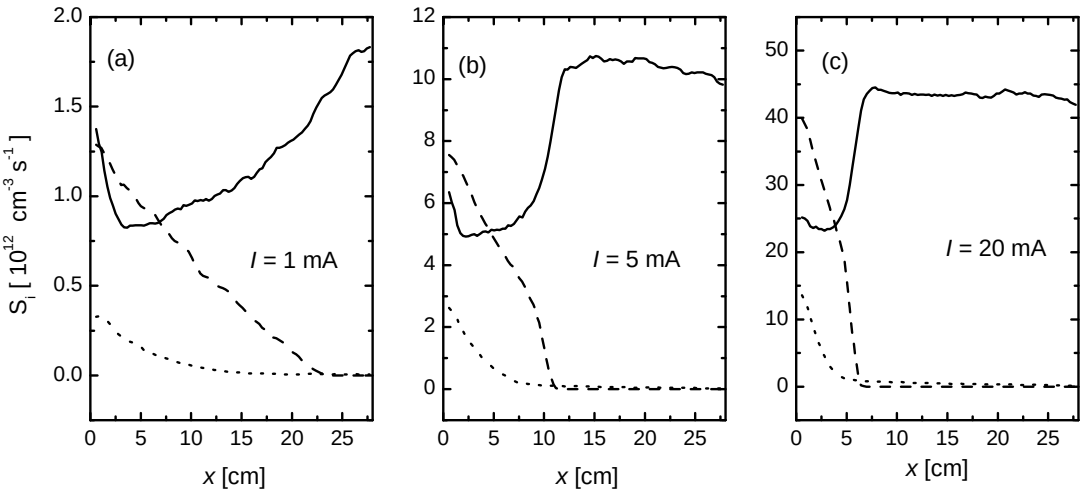

Figure 6. Contribution of electron impact (——), fast ion impact (– – –) and fast atom impact ($\cdots$) processes to the ionization source. ($V = 4000$ V, $L = 28$ cm, $I = 1$, 5 and 20 mA.)

The ionization source functions $S_i(x)$, shown in figure 6 for the 1, 5, and 20 mA cases, indicate that apart from the electron impact ionization, there is a significant source of ions due to the ionizing collisions between fast heavy particles and the background He atoms. Moreover, this latter part of the ionization source peaks near the cathode. This way the electrons created through this channel have a possibility to create additional electron avalanches, just like the primary electrons do. This effect strongly enhances the overall ionization rate in the discharge.

The importance of heavy particle ionization decreases with increasing discharge current. At 1 mA 32% of the ions are created in heavy particle processes. This part drops to 14 % at 20 mA. In lower voltage glow discharges the electron impact ionization rate (and similarly the electron impact excitation rate) peaks at (or very near) the cathode sheath – negative glow boundary [60] and decays nearly exponentially beyond this point [4]. In the present case we observe only a very slow decay of S_i in the negative glow. This shows that the electrode gap is too short

for the electrons to deposit their energy before reaching the anode, i.e. their energy relaxation length is much longer compared to the electrode distance.

It is interesting to note that as primary electrons leave the cathode they are soon accelerated to energies far exceeding the energy corresponding to the peak of inelastic cross sections. As a consequence of this many of the primary electrons fly through the cathode sheath and even the whole electrode gap without inelastic energy losses. Our calculations have confirmed that the spectrum of electrons at the anode shows a pronounced peak at the energy (4000 eV) corresponding to the full cathode fall voltage (beam electrons), in agreement with the experiments [53].

The apparent secondary electron emission coefficient at the cathode (as calculated by eq. (2)) is found to be $\gamma \approx 0.96$ for the investigated discharge conditions. This unusually high value of γ of course includes the contribution of fast atoms; for all discharge conditions investigated $\approx 75\%$ of the electrons are emitted from the cathode due to fast atom impact. The ratio of the fluxes of fast neutral atoms and ions at the cathode varies from about 10:1 for 1 mA to 8:1 for 20 mA. The secondary electron yield is approximately $\overline{\gamma}_{\mathrm{i}} = 0.24$ (in all cases) per 'average' ion and $\overline{\gamma}_{\mathrm{a}} = 0.072$ to 0.097 per fast atom, respectively. According to eq. (2) the contribution of fast atoms to the secondary emission is added to the contribution of the He^+ ions and this results in a high apparent secondary emission yield.

3.3. Light emission of argon discharges

The spatial distribution of light emission of glow discharges have been analyzed in several previous works. First we present representative results of Rózsa *et al* [4] regarding *spectrally resolved* measurements. In [4] intensity distributions have been recorded for an argon glow discharge established over a 4.3 cm diameter copper cathode mounted in a six-way metal cross that itself served as the anode. Results are presented here for 26.6 Pa pressure and four different spectral lines: the 476.5 nm Ar-II line, as well as the 451.1 nm, 750.3 nm, and 811.5 nm Ar-I lines. Representative spatial intensity distributions of these lines are presented in figure 7. The 476.5 nm Ar-II line is principally excited by electron impact, thus we only observe a pronounced negative glow. The distributions for the 411.5 nm and 750.3 nm atomic lines, on the other hand, recorded at the higher current values show a pronounced cathode glow, which is comparable in peak intensity to that of the negative glow. The intensity ratio of the cathode glow to that of the negative glow increases with increasing current (as analyzed in details in [4]), caused by the increased voltage. The 811.5 nm line is exceptionally sensitive to heavy particle excitation, here the cathode glow largely dominates the distributions at the highest currents.

The high sensitivity of this latter line to heavy-particle excitation also shows up in the distributions recorded by Kutasi and Donkó [61] using a plane-parallel hollow cathode discharge. Figure 8 reproduces light intensity distributions for this discharge, obtained at 60 Pa argon pressure and at 0.2 mA cm^{-2} current density (for more details see Ref. [61]). As hollow cathode discharges operate at reduced voltages compared to single plane cathode discharges, conditions for the development of the cathode glow are less favorable here. Nevertheless, besides the 811.5 nm line also the 750.3 nm line shows the feature characteristic for excitation by heavy particles.

To be able to analyze the contribution of heavy particles to excitation processes in more details, Marić *et al.* [62] have complemented the experiments by self-consistent discharge simulations based on a hybrid model described in section 2. In [62] the spatial distribution of the *integrated* light emission patters from argon glow discharges (operated with plane-parallel electrodes) have been measured for a wide range of discharge conditions. In the following, representative results of this work are presented here, for discharges operated at different pressures at a fixed value of $pd = 45$ Pa cm, with the electrode separation set to $d = 1.1$, 2.1 and 3.1 cm.

In the modeling study the cross sections of the elementary processes have been taken from

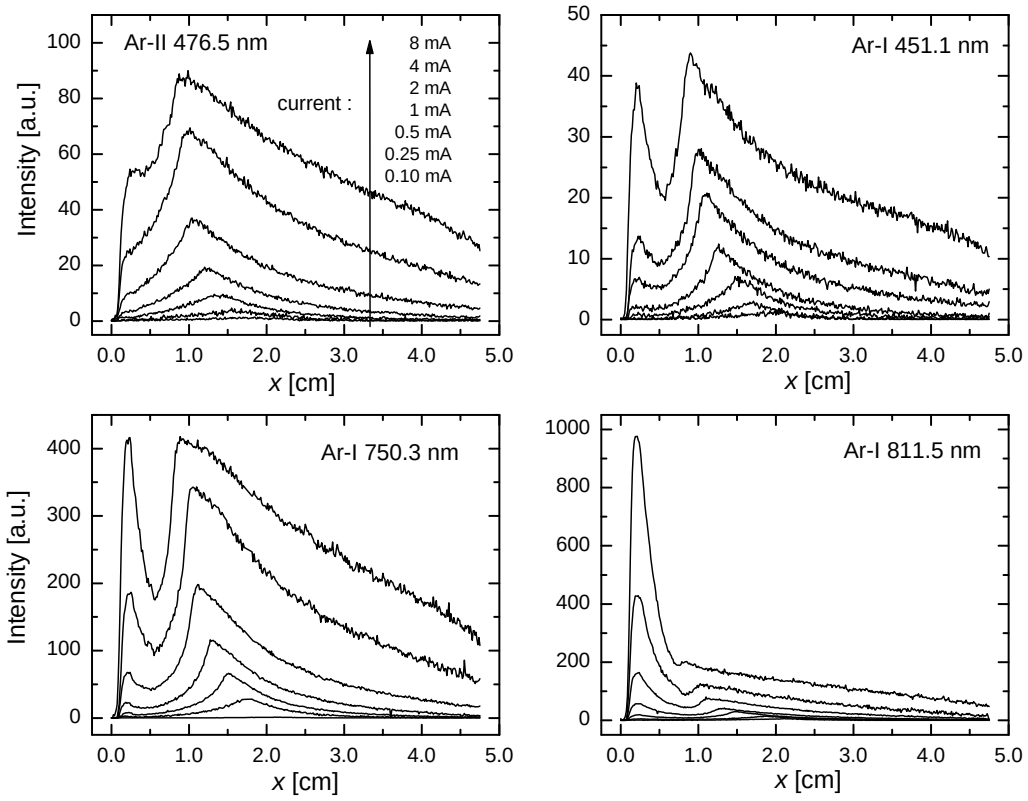

Figure 7. Spatial distributions of the intensities of selected argon spectral lines over a plane cathode surface at 26.6 Pa pressure [4]. All data have been taken at discharge currents given on the panel showing the intensity distributions of the 476.5 nm Ar-II line.

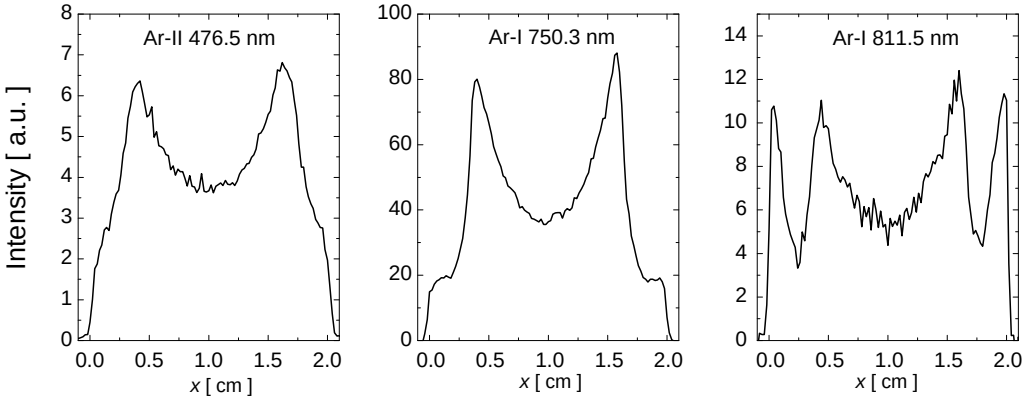

Figure 8. Spatial distributions of the intensities of selected argon spectral lines in a hollow cathode discharge [61] established between two flat cathode planes located at $x = 0$ and $x = 2$ cm. Discharge conditions: $j = 0.2$ mA cm^{-2} and $p = 60$ Pa.

Refs. [5, 6, 25], while the energy-dependent electron yield values of fast neutrals and ions, $\gamma_{\rm a}(\varepsilon)$ and $\gamma_{\rm i}(\varepsilon)$, respectively, (to be used in the calculation of the apparent electron yield) are from [2]. Data for surface processes are from [49, 50, 51, 52].

In figure 9 we show a comparison between the results of the model and the experimental light

intensity distributions [62]. The experimental and calculated intensity values have been scaled to match only at one selected value of the current, and this scale factor has been used subsequently for the normalization of all other calculated intensity data. The spatial profiles obtained by the model are in very good agreement with experiments, having in mind the uncertainties in the cross section data and the limitations of the model.

We clearly observe the formation of both the cathode glow (intensity peak close to the cathode) and the negative glow. The intensity of both of these features increases as the discharge current is increased. As the discharge conditions belong to the abnormal glow regime, the increase of current is accompanied with an increase of the voltage, so finally with an increase of the reduced electric filed E/n. In the low current regime (near the Townsend discharge) one observes only a small growth of excitation towards the cathode, as E/n is rather low for these conditions. The intensity ratio of the cathode glow to the negative glow increases as the current is increased.

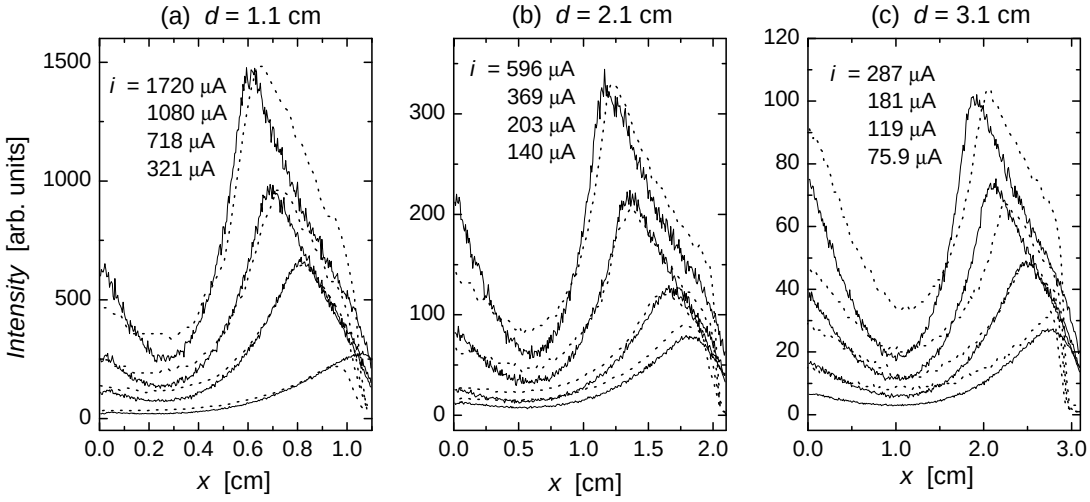

Figure 9. Comparison of experimental (- - - -) and calculated (——) profiles of spectrally integrated light emission of argon glow discharges with plane-parallel electrodes separated by (a) d=1.1 cm; (b) d= 2.1 cm; (c) d= 3.1 cm [62].

The excitation rate of Ar atoms is decomposed into contributions due to electron and heavy-particle impact in Fig. 10(a). At these conditions heavy-particle excitation plays an important role near the cathode. Similarly to the excitation processes, at high E/n values heavy-particle ionization also becomes important. The "additional" electrons created via this process – as they are created near the cathode – behave almost like the electrons emitted from the cathode and have the potential to create further electron avalanches. This way the Ar^F + Ar and Ar^+ + Ar collisions greatly enhance the overall ionization and excitation rates. The effectiveness of heavy-particle processes is found to depend strongly on the strength of the reduced electric field E/n. This is illustrated in figure 10(b) where the normalized heavy-particle excitation rate $S^*(x)$ at the cathode is plotted against E/n at the cathode surface, $(E/n)_c$. The excitation rate is normalized by taking into account the dependence of current density on pressure (j/p^2 scaling) and the similarity law for length scaling. The data obtained from the simulation of the discharges with different electrode separations show a universal behavior independently of the electrode separation.

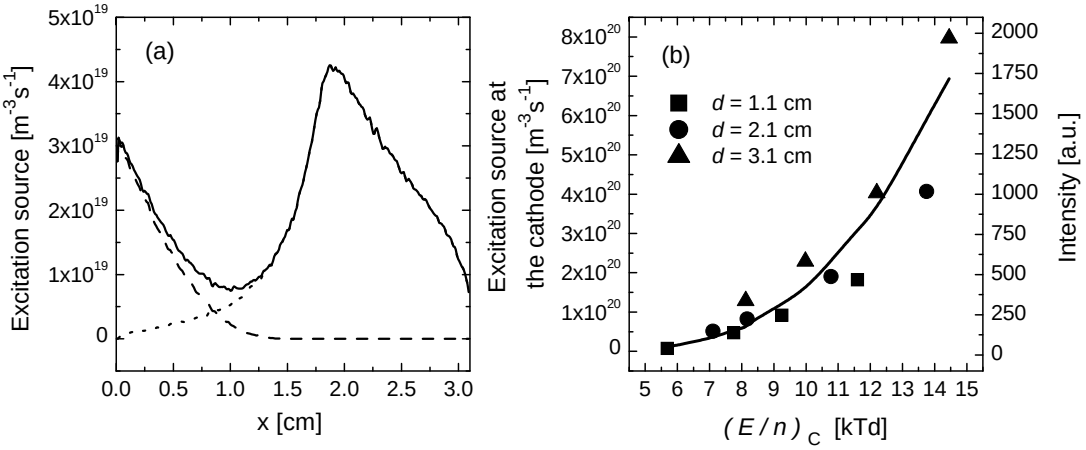

Figure 10. (a) Contributions of electron impact ($\cdots$) and heavy-particle impact ($- - -$) collisions to excitation of gas atoms. The total excitation rate is shown by the solid line. Discharge conditions: d= 3.1 cm, V = 510 V. (b) Normalized heavy-particle excitation rate near the cathode as a function of the reduced electric field at the cathode. The solid curve is a fit to the results of the simulation, the symbols indicate experimental data [62].

4. Conclusions

This paper intended to review some of the prominent effects of fast heavy particles on the characteristics of low-pressure noble gas discharges. The experimental data, as well as the results of numerical simulations indicate that heavy particles contribute significantly to both surface (electron emission) and gas-phase (charged particle creation and excitation) processes when the reduced electric field is sufficiently high. Under these conditions, which can favorably be reached at high discharge voltages and at low pressures, it is advisable to consider heavy particle processes in discharge models in order to give a more precise description of the physics of these discharges.

Acknowledgments

This work has been supported by the Hungarian Scientific Research Fund through the grants OTKA-T-48389 and OTKA-PD-049991.

References

[1] Francis G 1956 *The Glow Discharge at Low Pressure*, Encyclopedia of Physics, ed Flügge S, Springer Verlag
[2] Phelps A V and Petrović Z Lj 1999 *Plasma Sources Sci. Technol.* **8** R21
[3] Malović G, Strinić A, Živanov S, Marić D, Petrović Z Lj 2003 *Plasma Sources Sci. Technol.* **12** S1
[4] Rózsa K, Gallagher A, Donkó Z 1995 *Phys. Rev. E* **52** 913
[5] Phelps A V, Collision data compilation, http://jilaweb.colorado.edu/www/research/colldata.html
[6] Phelps A V 1991 *J. Phys. Chem. Ref. Data* **20** 557
[7] Phelps A V 2001 *Plasma Sources Sci. Technol* **10** 329
[8] Revel I, Pitchford L C, Boeuf J P 2000 *J. Appl. Phys.* **88** 2234
[9] Bogaerts A, Gijbels R, Serikov V V 2000 *J. Appl. Phys.* **87** 8334
[10] Donkó Z, *Phys. Rev. E* 2001 **64** 026401
[11] Bogaerts A, Gijbels R 2004 *J. Anal. At. Spectrom.* **19** 1206
[12] Csillag L, Jánossy M, Rózs K, Salamon T 1974 *Phys. Lett.* **50A** 13
[13] Tobin R C, Peard K A, Bode G H, Rózsa K, Donkó Z, Szalai L 1995 *IEEE J. of Selected Topics in Quant. Electron.* **1** 805
[14] Mihailova D B, Grozeva M, Bogaerts A, Gijbels R, Sabotinov N V 2003 *Proc. SPIE* **5226** 49
[15] Walsh A 1956 *Spectrochimica Acta* **7** 108

[16] Payling R, Jones D, Bengtson A (editors) 1997 *Glow Discharge Optical Emission Spectrometry*, John Wiley & Sons, Chichester
[17] Pitchford L C, Boeuf J P, Segur P, Marode E 1990 *Nonequilibrium Effects in Ion and Electron Transport*, ed. Gallagher J W (Plenum Press, New York)
[18] Bogaerts A, Gijbels R, Goedheer W J 1996 *Anal. Chem.* **68** 2296
[19] Serikov V V, Nanbu K 1997 *J. Appl. Phys.* **82** 5948
[20] Bogaerts A, Gijbels R, Serikov V V 2000 *J. Appl. Phys.* **87** 8334
[21] Donkó Z 2000 *J. Appl. Phys.* **88** 2226
[22] Yoshida S, Phelps A V, Pitchford, L C 1983 *Phys. Rev. A* **27** 2858
[23] Opal C B, Peterson W K, Beaty E C 1971 *J. Chem. Phys.* **55** 4100
[24] Boeuf J-P, Marode E 1982 *J. Phys. D* **15** 2169
[25] Phelps A V 1994 *J. Appl. Phys.* **76** 747
[26] Bogaerts A, van Straaten M, Gijbels R 1995 *Spectrochim. Acta* **50B** 179
[27] Abril I, Gras-Marti A, Valles-Abarca J A 1984 *J. Phys. D* **17** 1841
[28] Boeuf J-P, Pitchford L C 1991 *IEEE Trans. Plasma Sci.* **19** 286
[29] Fiala A, Pitchford L C, Boeuf J-P 1994 *Phys. Rev. E* **49** 5607
[30] Donkó Z, Hartmann P, Kutasi K 2006 *Plasma Sources Sci. Technol.* **15** 178
[31] Bánó G, Hartmann P, Kutasi K, Horváth P, Plašil R, Hlavenka P, Glosík J, Donkó Z 2006 Combined Langmuir probe, electrical and hybrid modeling characterization of glow discharges, submitted to *Plasma Sources Sci. Technol.*
[32] Winters H F, Coufal H, Retter C T, Bethune D S 1990 *Phys. Rev. B* **41** 6240
[33] Coufal H, Winters H F, Bay H L, Eckstein W 1991 *Phys. Rev. B* **44** 4747
[34] Penning F M 1931 *Proc. Roy. Acad. Amst.* **34** 1305
[35] Meek J M, Craggs J D 1953 *Electrical Breakdown of Gases* Clarendon Press, Oxford
[36] Ward A L, Jones E 1961 *Phys. Rev.* **122** 376
[37] Guseva L G 1964 in *Investigations into Electrical Discharges in Gases*, ed Klyarfeld B N, Macmillan, New York.
[38] Auday G, Guillot Ph, Galy G, Brunet H 1998 *J. Appl. Phys.* **83** 5917
[39] Jelenković B M, Phelps A V 1998 *Bull. Am. Phys. Soc.* **43** 1432
[40] Hartmann P, Donkó Z, Bánó G, Szalai L, Rózsa K 2000 *Plasma Sources Sci. Technol.* **9** 183
[41] Nickel J C, Imre K, Register D F, Trajmar S 1985 *J. Phys. B* **18** 125
[42] de Heer F J, Jansen R H J 1977 *J. Phys. B* **10** 3741
[43] Cramer W H, Simons J H 1985 *J. Chem. Phys* **26** 1272
[44] Okasaka R, Konishi Y, Sato Y, Fukuda K 1987, *J. Phys. B* **20** 3771
[45] Gilbody H B, Hasted J B 1957 *Proc. Roy. Soc. A* **240** 382
[46] Jordan J E, Amdur I 1967 *J. Chem. Phys* **46** 165
[47] Kempter V, Veith F, Zehnle L 1975 *J. Phys. B* **8** 1041
[48] Hayden H C, Utterback N G 1964 *Phys. Rev.* **135** A1575
[49] Myers H P 1952 *Proc. Roy. Soc. A.* **215** 329
[50] Harrower G A 1956 *Phys. Rev.* **104** 52
[51] Darlington E H, Cosslett V E 1972 *J. Phys. D* **5** 1969
[52] Jardin C, Kessas S, Khelifa B, Bondott P, Gruzza B 1991 *J. Phys. D* **24** 1115
[53] Fukao M, Ishida M, Ohtsuka Y, Matsuo H 2000 *Vacuum* **59** 358
[54] Matsuo H, Ohtsuka Y, Fukao M 2002 *Proc. ESCAMPIG-16/ICRP-5 Conf.*, Grenoble, France, 2002, Vol. 2, p. 73.
[55] Sari A H, Ghoranneviss M, Hora H, Osman F, Höpfl R, Hantehzadeh M R, Bolouki N, 2004 *J. Plasma Fusion Res.* **6** 735
[56] Hartmann P, Matsuo H, Ohtsuka Y, Fukao M, Kando M, Donkó Z 2003 *Jpn. J. Appl. Phys.* **42** 3633
[57] Donkó Z, Rózsa K, Tobin R C, Peard K A 1994 *Phys. Rev. E* **49** 3283
[58] Boeuf J-P, Pitchford L C 1995 *J. Phys. D* **28** 2083
[59] Ohtsuka Y, unpublished.
[60] Marić D, Kutasi K, Malović G, Donkó Z, Petrović Z Lj 2002 *Eur. Phys. J. D* **21** 73
[61] Kutasi K, Donkó Z 2000 *J. Phys. D* **33** 1081
[62] Marić D, Hartmann P, Malović G, Donkó Z, Petrović Z Lj 2003 *J. Phys. D* **36** 2639